MSc in Photonics

Universitat Politècnica de Catalunya (UPC)
Universitat Autònoma de Barcelona (UAB)
Universitat de Barcelona (UB)
Institut de Ciències Fotòniques (ICFO)

PHOTONICS**BCN**

http://www.photonicsbcn.eu

Master in Photonics

MASTER THESIS WORK

CHARACTERIZATION OF A QUANTUM FREQUENCY CONVERTER FOR QUANTUM REPEATER APPLICATIONS

Xavier Fernandez Gonzalvo

Supervised by Prof. Hugues de Riedmatten, (ICFO)

Presented on date 3rd September 2012

Registered at

Escola Tècnica Superior d'Enginyeria de Telecomunicació de Barcelona

Characterization of a quantum frequency converter for quantum repeater applications

Xavier Fernandez-Gonzalvo

ICFO - Institut de Ciències Fotòniques, Mediterranean Technology Park, 08860 Castelldefels (Barcelona), Spain

E-mail: xavier.fernandez@icfo.es

Abstract. Quantum frequency conversion of quantum memory compatible photons to telecom wavelength is a requirement for the implementation of scalable quantum repeaters, a key ingredient for long distance quantum communications in optical fibers. In this work we characterize a quantum frequency converter implemented with a non-linear waveguide, meant to be coupled to a rubidium atomic ensemble quantum memory. We show promising results allowing us to work in the quantum regime, being this the first demonstration of quantum frequency conversion with quantum memory compatible photons using a solid state device.

Keywords: quantum frequency conversion, quantum repeater, nonlinear optics.

1. Introduction

Quantum communication is the art of transmitting quantum information over long distances. In classical communication the common way of transferring information between two distant places is to send pulses of light through optical fibers. Due to the exponential damping of the signal, in a typical fiber 99% of the signal is lost after 100 km. The solution for this is to place a series of repeaters along the fiber, commonly every 50-100 km, which are devices that amplify the signal by copying it and sending it along with the original one. A fundamental characteristic of the nature of quantum states is that, due to the no cloning theorem [1], they can not be copied, so the classical solution does not work for quantum communications. A proposal to solve such a problem is to use quantum repeaters [2], which are based on entanglement. Entanglement is a fundamental resource in quantum communication which leads to non-classical correlations between remote particles. Distributing a pair of entangled particles over long distances is an important process since it can be used for quantum teleportation or quantum key distribution amongst others.

1.1. Quantum repeaters

Quantum repeaters are (still theoretical) systems that will allow us to share entanglement between two distant particles. The basic process is to split the

total distance in several links, distribute entanglement in each link and extend the entanglement distance using entanglement swapping. The distribution of entanglement within each link, though, is a probabilistic process, and this makes the time required to entangle the whole chain to scale exponentially with the number of segments. This problem is solved if one has a device capable of storing a quantum state, i.e. a quantum memory (QM). One of the most successful proposals for achieving this goal is the DLCZ protocol [3] which we summarize in figure 1. The QMs A and C1 are excited by a common coherent pump and they emit a photon (Stokes) which is strongly correlated with a spin excitation in the ensemble. This photon travels towards the detector couple D1 passing through a beam splitter, so when one of these detectors clicks we have no way to know from which memory it came. This projects A and C1 into an entangled state, and the entanglement is stored in the quantum memories. In the other side B is entangled with C2 in a similar way with the D2 detectors. Then by performing an entanglement swapping operation with memories C1 and C2 using the detectors in D3 one can leave A entangled with B. Such a process would make the repeater scalable, i.e. with a sub exponential scaling with time.

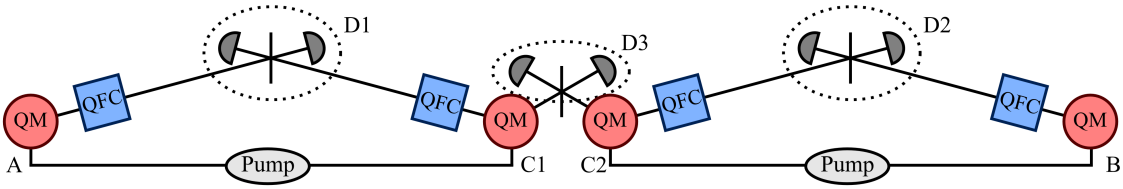

Figure 1. Schematic representation of the setup performing the DLCZ protocol.

Several systems have been proposed to implement a QM [2], for example atomic ensembles of rubidium or cesium atoms working at 780 nm and 852 nm wavelength respectively, or rare earth doped crystals like prosedimium working at 606 nm. On the other hand optical fibers for telecommunications have the lowest transmission loss for wavelengths in the range from 1530 nm to 1565 nm (the so called C-band). This creates the need for a device capable of transforming a photon at a given wavelength into a photon suitable for propagation into an optical fiber. Such a device is what we call a quantum frequency converter (QFC) (see figure1).

1.2. The Quantum Frequency Conversion experiment

In our case we dispose of an experimental quantum memory based on rubidium atoms working at a wavelength of 780 nm. This type of atomic ensemble has proven to be one of the best quantum memories to date [4, 5]. Our final goal will be then to convert the wavelength of these photons to 1550 nm while preserving their quantum properties.

The frequency conversion is performed via difference frequency generation (DFG) which is a second order nonlinear process involving three wave mixing in such a way that, by energy conservation, $\omega_s = \omega_i - \omega_p$, where ω_i (idler) is the frequency corresponding to

the photons we intend to convert (λ_i=780.24 nm), ω_s (signal) is the one corresponding to the converted photons (λ_s around 1550 nm) and ω_p (pump) is the one corresponding to the auxiliary beam we will use in the process (λ_p=1569.0 nm). With these numbers:

$$\lambda_s = \frac{1}{\frac{1}{\lambda_i} - \frac{1}{\lambda_p}} = 1552.05\, nm. \tag{1}$$

In our experiment we use a periodically poled potassium titanyl phosphate (PP-KTP) waveguide acting as the nonlinear medium, and in order to conserve momentum the quasi phase matching condition must be also fulfilled. We work in collinear propagation configuration, implying this that we must send the idler and pump beams overlapping each other at the input of the waveguide, and that at the output we have a superposition of signal, idler and pump propagating along the same direction, so a filtering stage is required. This makes the experiment itself quite challenging, since one must be able to distinguish a single photon from the background noise, which can be originated from different sources. Since the pump beam is only 20 nm away from the signal there can be some leakage in the filtering stages, or even the pumping laser can emit some light at 1550 nm. Another noise source can be Raman scattering in the waveguide, in such a way that some of the pump photons at 1570 nm are converted into 1550 nm photons and mixed with the signal.

The experimental approach is to start by converting a beam at 780 nm coming from a continuous wave laser, then create artificial pulses of light with a certain mean number of photons μ (recall the Poissonian statistics for classical pulses of light) and then decrease μ as much as possible, ideally until much less than 1, always keeping a signal to noise ratio (SNR) above 1. The figure of merit of our experiment will be then the mean number of photons μ_1 required to have SNR=1.

Quantum frequency conversion at the single photon level from visible to telecom wavelength has been demonstrated in a few experiments recently [6–10], but so far never with QM compatible photons.

The present experiment was the subject of a previous Master thesis at ICFO [11], and the best results achieved show μ_1=120. Thanks to the filtering system designed it was possible to show that the noise detected is not due to pump leakage or the pump laser emitting at 1550 nm. The aims of the current project will be then the following:

- **Characterize the noise:** check if the main source of noise is indeed Raman noise and try to reduce it.
- **Characterize the filtering stage:** check if by reducing the bandwidth of the filtering stage one can decrease the noise level while keeping the same signal, thus increasing the SNR.
- **Reduce the mean number of photons:** find mechanisms to decrease the mean number of photons per pulse required to have SNR=1, ideally getting into the quantum regime ($\mu_1 << 1$).

2. Experimental methods and results

2.1. Experimental setup

In figure 2 we show a simplified scheme of the experimental setup. The idler laser (780 nm) is an external cavity diode laser locked on the ^{87}Rb D2 line at 780.24 nm. We send its light to an acousto-optic modulator in double passage (AOMx2) that allows us either to send a beam in continuous wave or to generate light pulses. The half wave-plate (HWP1) and the polarizing beam splitter (PBS) in front of the AOM line allow us to control the 780 nm power. This light is then coupled into a fiber and sent to the second stage of the experiment in which we overlap it with the pump beam (1570 nm), that comes from a tunable laser typically fixed at 1569.0 nm connected to an erbium doped fiber amplifier (AMP). The pump beam passes through a polarization controller (PC1) that helps to increase the efficiency of the diffraction grating (DG1) used to spectrally filter the light, ensuring this way that we will see no 1550 nm photons coming from the pump. Then it is coupled again into a fiber and overlapped with the 780 nm beam with the help of a dichroic mirror (DM). Both beams are then coupled into the waveguide (WG) using an aspheric lens of 11 mm focal length (L1). The WG is a 2.6 cm PP-KTP crystal with a poling period of 19.9 μm and with a normalized efficiency for DFG of around 38%/W. HWP2 and PC2 are used to set the right polarization for the WG in order to achieve maximal conversion efficiency, which is measured to be around 6% for the power we use. Inside the WG the signal is generated via DFG, and at the output the three beams (signal, idler and pump) are collimated with the help of L2. The signal filter (SF) blocks the 780 and the 1570 beams having a transmission window that ranges from approximately 1545 nm to 1554 nm. DG2 is used to further filter the signal, where HWP3 is used to optimize the diffraction efficiency. After that the signal beam is coupled into a fiber that brings the light to an InGaAs single photon avalanche detector (SPAD). This type of detector works in gated mode, i.e. it is active only during a short period of time τ. The SPAD and the AOM are synchronized by a digital delay generator (DDG).

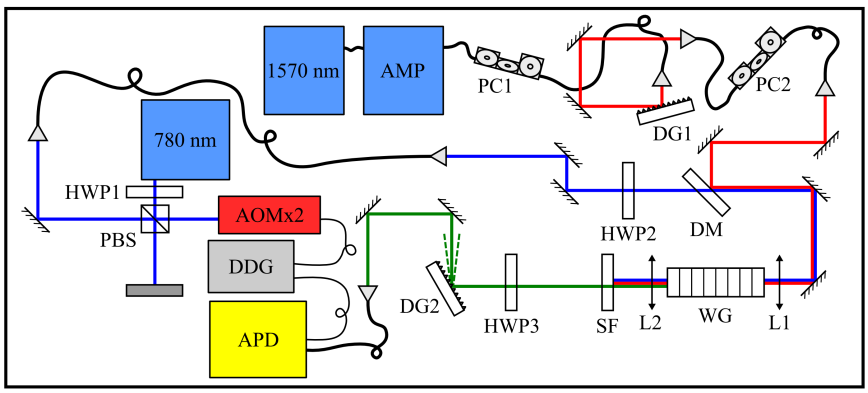

Figure 2. Experimental setup.

2.2. Pulse measurements

To understand a typical measurement in our experiment it is important to understand what we see when we look at the SPAD. In the first stage, to simulate photons coming from the ^{87}Rb atomic ensemble, we generate pulses with a temporal width of 30 ns, which is approximately the life-time of the atomic transition of interest. Then we have to set a τ in the SPAD suitable for this, and typically we will choose it to be of 20 ns. After choosing the detection width we have to synchronize the SPAD with the arrival of the pulses with the DDG. To see what are we exactly measuring when doing this we choose momentarily the biggest detection gate possible (100 ns) and take an arrival time histogram measurement to see the shape of the pulse. The results are shown in figure 3.a), where in the horizontal axis we have the time in units of the full width half maximum (FWHM) of the signal pulse and in the vertical we have detector counts normalized to the noise level, which we will explain next. The green constant line indicates the dark counts (DC) which are inherent to the detector. We can measure the DC level just by blocking all the light coming to the detector. The blue line represents the noise counts (N) plus the dark counts. N+DC is measured by blocking the 780 nm beam, so what we observe is the noise produced by the pump laser that passes through the different filters of the experiment. Finally the red curve is the sum of the signal (S) the noise and the dark counts. The vertical lines indicate the usual 20 ns gate for pulses of 30 ns FWHM corresponding to the normalized time $t^* = \frac{\tau}{FWHM} = 0.66$.

Now we define SNR as the ratio between the area under the signal and the noise curves inside of the chosen τ:

$$SNR = \frac{\int_\tau S\,\mathrm{d}t}{\int_\tau N\,\mathrm{d}t} \tag{2}$$

where the dark counts are not taken into account because they are a technical artifact that do not depend on the conversion process. We can define now the effective detection

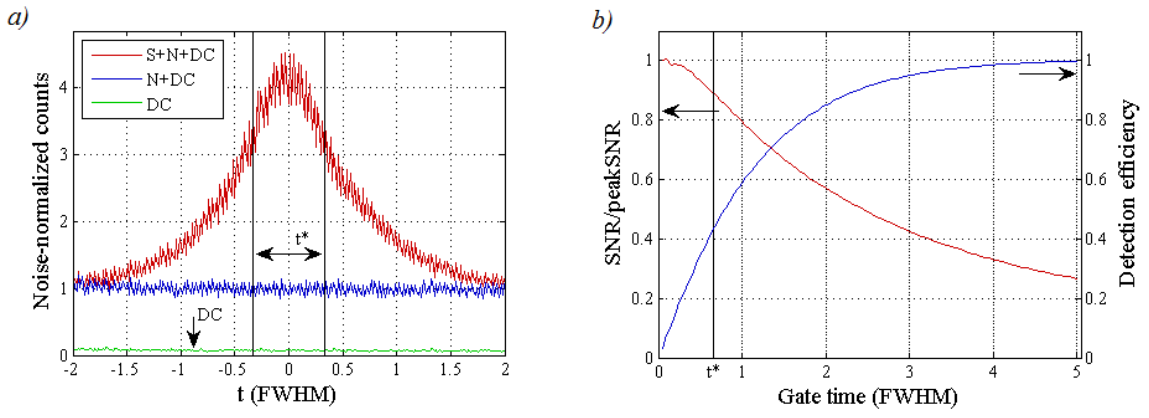

Figure 3. *a)* Histogram measurements for the signal (S), the noise (N) and the dark counts (DC) for $\mu = 16$ and a pump power coupled into the WG of 107 mW. *b)* Dependence of the SNR and the detection efficiency as a function of the detection gate time.

efficiency as the ratio between the integral of the detected signal over the whole signal:

$$D_{eff} = \frac{\int_{\tau} S\,\mathrm{d}t}{\int_{-\infty}^{+\infty} S\,\mathrm{d}t}\,. \tag{3}$$

We see that by decreasing τ we increase SNR but at the same time we decrease D_{eff}, so we have to get to a compromise between these two. In figure 3.b) we show how this two parameters change, where the red curve represents the SNR normalized to the SNR we would have for $\tau \to 0$ and the blue one represents the detection efficiency.

2.3. Dependence of the SNR with the filtering width

Now we want to study how the filtering bandwidth affects the SNR, to check if a narrower filter implies a lower level of noise while keeping the same amount of signal. There exist a dependence of the filtering width with the transversal shape of the signal beam in such a way that for vertical shapes the filtering is narrower than for horizontal shapes. The explanation for this fact is that since we use a diffraction grating to filter, that separates the different wavelengths in the horizontal plane, if one uses horizontally shaped beams the different spectral components overlap more than if one uses vertically shaped beams. The transversal shape can be modified by changing the longitudinal position of the output lens L2. In figure 4.a) we can observe different transmission curves for different beam shapes and the corresponding filtering widths. The wider one (in red) corresponds to a horizontally shaped beam whilst the narrower one (blue) is for a vertically shaped beam. The central curve (yellow) corresponds to a circular beam, and we plotted also two intermediate cases (orange and green). The difference between the best and the worst case is quite significant, ranging from 0.6 nm to 4.0 nm FWHM. There appears an extra effect that we are not able to explain consisting of a shift of the central frequency, which is of high relevance since it modifies the transmission for the signal (at 1552 nm). The change in the beam shape also modifies slightly the efficiency of the diffraction grating and the coupling to the optical fiber. In figure 4.b we present

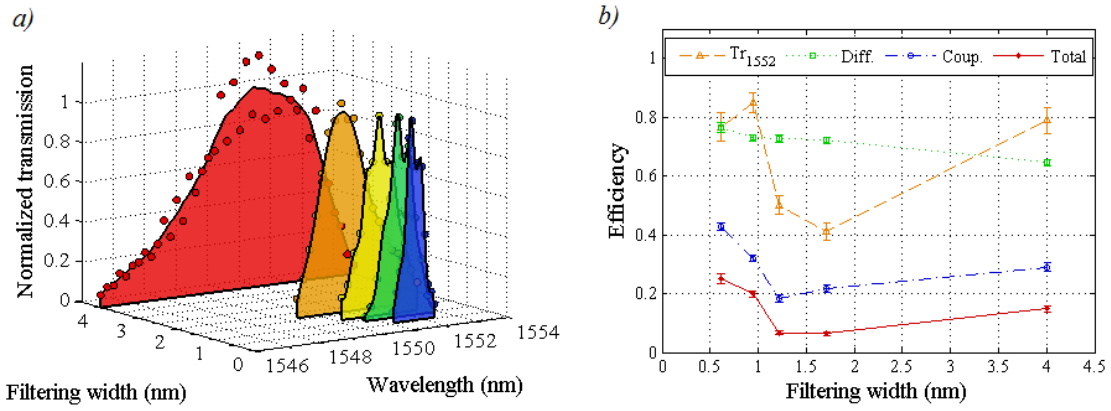

Figure 4. *a)* Normalized transmission curves of the filtering stage for different beam shapes. *b)* Different efficiencies of the filtering stage for different filtering widths.

how these parameters change as a function of the corresponding filtering width, where the yellow dashed line is the transmission at 1552 nm, the green dotted line is the diffraction efficiency, the blue dot-dashed line is the coupling efficiency and the red solid line is the total efficiency, equal to the product of all the previous parameters. As we can observe the total efficiency has a minimum at the center. This causes some troubles when aligning the setup because when doing so one tries to maximize the signal, and starting with a circular beam it is extremely easy to end up going towards wider filtering widths.

The next step is to study how the filtering width affects μ_1. In figure 5.a) we show the results of such study, conducted by measuring the SNR for different μ and for different filtering widths. The graphic in logarithmic scales shows how we can decrease μ_1, starting by the rightmost curve (red) corresponding to 4.0 nm bandwidth to the leftmost one (blue) corresponding to 0.6 nm. In figure 5.b) we see more clearly how μ_1 decreases with the filtering bandwidth. We can extract from the measurement that the noise is broadband, which is an expected characteristic of Raman noise.

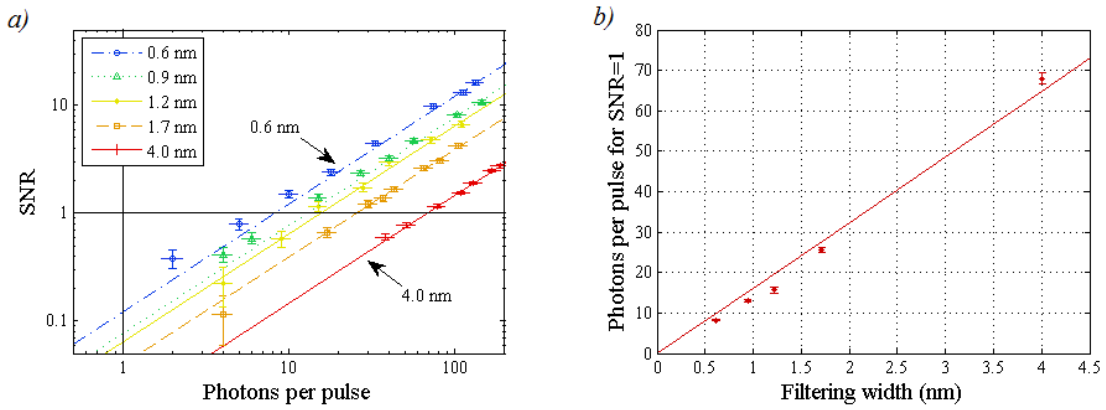

Figure 5. *a)* SNR as a function of μ for different filtering widths. *b)* μ_1 as a function of the filtering width.

2.4. Dependence of the SNR with the pump wavelength

Using the tunable laser we are able to scan the pump wavelength with the intention to see if we are in a Raman peak of noise and if there is a better wavelength at which we can work. In figure 6.a) we show the measurements of μ_1 in a scanning range from 1567.0 nm to 1569.5 nm, taking points every 0.5 nm. Indeed for different pump wavelengths we have a different noise level which is a characteristic feature of Raman noise. Finally to ensure that this result is not an artifact produced by a possible change of the filtering width when changing the pump wavelength we perform the corresponding transmission measurements, shown in figure 6.b). We can appreciate how the filtering bandwidth is practically constant, and so we can conclude that there is a noise peak around 1568 nm which should be avoided.

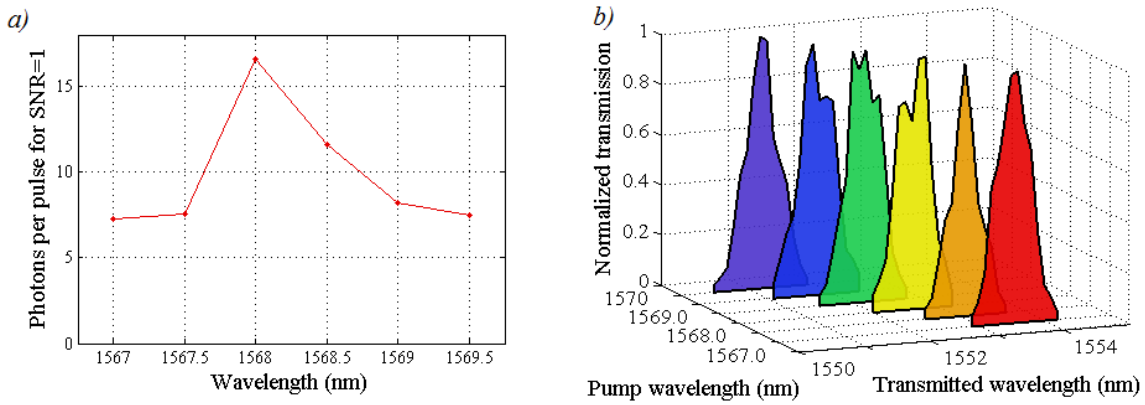

Figure 6. *a)* μ_1 as a function of the pump wavelength. *b)* Normalized transmission curves for different pump wavelengths.

2.5. Polarization study

To finish with the characterization we would like to further analyze the noise and to see if we can filter it by polarization means. With the help of an extra half wave-plate and a polarizing beam splitter placed at the output of the WG we are able to study the polarization of both signal and noise separately. The results as a function of the angle of the wave plate θ are shown in figure 7 where the signal is represented by the red dotted line and the noise by the blue dashed one. Superimposed we have a sinusoidal fit for both cases. In the bottom plot we see the SNR in green, fitted by the quotient of the previous sinusoidal fits. The data show how the signal, with a visibility of 0.95, is completely polarized, which is to be expected. The noise, in contrast, with a visibility of 0.72, is not totally but mostly polarized, feature that can also be seen in the SNR plot since for S and N equally polarized we would expect a flat line. Filtering the signal by polarization means, however, would not result in a substantial improvement.

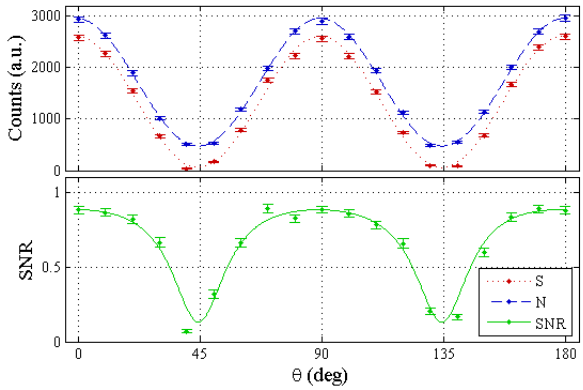

Figure 7. *Top:* signal (S) and noise (N) counts as a function of the polarization angle θ. *Bottom:* behavior of the SNR with respect to θ.

3. Discussion about the noise

We have seen that the noise is broadband and that it depends on the pump wavelength. This is consistent with Raman noise. In figure 8.a) we show a superimposed image of figure 6.a) over the Raman spectrum for bulk KTP [12]. We can appreciate how the shape of the peak at 1568 nm is in accordance with the data, even though there is a frequency shift. This shift may be possibly partly explained by the fact that we don't know the absolute calibration of the tunable laser. Moreover some discrepancies are to be expected since we work in a waveguide and the study of [12] is done in bulk crystal. On top of the same figure we plot the dependence of the noise with the pump power, where the horizontal dashed line marks the dark counts level. As we can see the noise increases linearly with the power as it would be expected, since Raman scattering is a linear process. All this information strongly supports the hypothesis of Raman noise.

4. PP-LN waveguide

Towards the end of the stay we received a new waveguide made of a periodically poled lithium niobate crystal (PP-LN) which in principle is much more efficient than PP-KTP. In only one week, and thanks to all the experience previously obtained, we could achieve much better results than with the old one. In figure 8.b) we show a comparison of both materials, where the blue line represents the best result obtained with the PP-KTP and the red dashed line represents the new results with the PP-LN. With this new waveguide we passed from $\mu_1 = 8.2$ to μ_1=0.13, way into the quantum regime, but some more improvement can still be done.

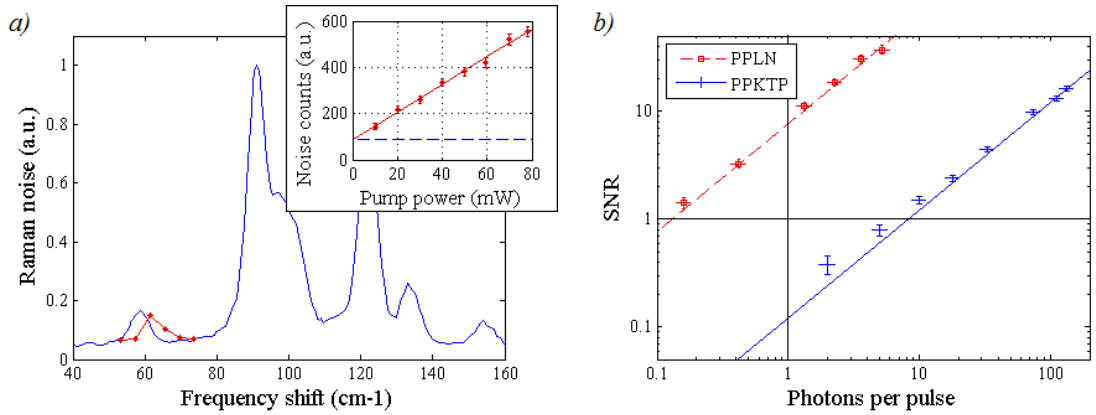

Figure 8. *a)* Qualitative comparison between our data and the Raman spectrum for bulk KTP [12] and noise dependence with the pump power showing a linear behavior. *b)* Comparison of the SNR as a function of the mean number of photons per pulse between the old PP-KTP and the new PP-LN waveguides.

5. Conclusions and future directions

In this work we have studied the noise generated in the difference frequency generation of a weak pulse from 780 nm to 1550 nm, using a strong pump at 1569 nm. We have also shown how we can reduce the required number of photons per pulse in order to have SNR=1 by decreasing the filtering bandwidth. Thanks to this we were able to reduce this number from an original 120 photons per pulse to slightly more than 8 with the PP-KTP waveguide and to 0.13 with the PP-LN one, which still holds some room for improvement. This last result represents the first demonstration of quantum frequency conversion with quantum memory compatible photons realized with a solid state device. Taking these results into account we have plans to insert an ultra narrow-band Bragg diffraction fiber filter which should help to increase the SNR by more than an order of magnitude. Then once the system is efficient enough we can connect it to the rubidium quantum memory and work with real single photons, and proceed to check if the quantum properties are conserved after the frequency conversion.

Acknowledgments

I would like to thank Prof. Hugues de Riedmatten for giving me the opportunity of developing my master thesis in the Quantum Photonics with Solids and Atoms group at ICFO. Special mention to Matteo Cristiani for his invaluable teachings and support, and to all the members of the QPSA group who helped me throughout my experience. Thanks also to Valerio Pruneri's group at ICFO for lending us the tunable laser.

References

[1] W.K. Wootters, W.H. Zurek, Nature 299, pp. 802803 (1982).
[2] N. Sangouard, C. Simon, H. de Riedmatten, N. Gisin, Rev. Mod. Phys. 83, 3380 (2011).
[3] L.-M. Duan, M. D. Lukin, J. I. Cirac, P. Zoller, Nature (London) 414, 413 (2001).
[4] A. G. Radnaev, Y. O. Dudin, R. Zhao, H. H. Jen, S. D. Jenkins, A. Kuzmich, T. A. B. Kennedy, Nature Physics, 894-899 (2010).
[5] X. Bao, A. Reingruber, P. Dietrich, J. Rui, A. Dück, T. Strassel, L. Li, B. Zhao, J. Pan, Nature Physics, vol. 8, pag. 517 (2012).
[6] N. Curtz, R. Thew, C. Simon, N. Gisin, H. Zbinden, Optics Express, Vol. 18, Issue 21, pp.22099-22104 (2010).
[7] H. Takesue, Phys. Rev. A, 82, 013833 (2010).
[8] S. Zaske, A. Lenhard, C. Becher, Optics Express, Vol. 19, Issue 13, pp. 12825-12836 (2011).
[9] R. Ikuta, Y. Kusaka, T. Kitano, H. Kato, T. Yamamoto, M. Koashi, N. Imoto, Nature Communications, 2, 537 (2011).
[10] S. Zaske, A. Lenhard, C. A. Kessler, J. Kettler, C. Hepp, C. Arend, R. Albrecht, W. Schulz, M. Jetter, P. Michler, C. Becher, arXiv:1204.6253 (2012).
[11] G. Corrielli, Tesi di Laurea, Politecnico di Milano (2011).
[12] I. Savatinovay, I. Savovay, E. Liarokapisz, C. C. Zilingx, V. V. Atuchinx, M. N. Armenisek, V. M. N. Passarok, J. Phys. D: Appl. Phys. 31 1667 (1998).